Electric field gradient of Pt, Ir, Os, and Re in cubic cobalt

G. Seewald, E. Hagn, and E. Zech
Physik-Department, Technische Universität München, D-85748 Garching, Germany
(Received 11 August 2000; published 11 January 2001)

The electric quadrupole interaction of ^{181}Re, ^{183}Os, ^{186}Ir, and ^{191}Pt in polycrystal samples of cubic Co has been measured using modulated adiabatic fast passage on oriented nuclei. The average electric field gradients of Re, Os, Ir, and Pt in cubic Co were deduced to be $+0.36(26)$, $-1.15(11)$, $-1.04(5)$, and $+0.23(5)$ 10^{16} V/cm^2, respectively. These results are compared with the spin-orbit induced electric field gradients of $5d$ impurities in Fe, Ni, and hexagonal Co. In addition the hyperfine field of Re in cubic Co has been determined to be $-48.4(2)$ T and the difficulties in deducing the intrinsic electric field gradient from strongly inhomogeneously broadened field gradient distributions are discussed.

DOI: 10.1103/PhysRevB.63.054428 PACS number(s): 76.60.Jx, 75.50.Cc, 76.60.Gv, 76.80.+y

I. INTRODUCTION

The electric field gradient (EFG) at the nuclear site is a measure for the deviation of the surrounding electron charge distribution from cubic symmetry. Therefore, in solid matter the EFG is usually connected with a noncubic lattice symmetry around the respective nucleus. However, in ferromagnetic Fe, fcc Co, and Ni the lattice symmetry is cubic and the EFG is a consequence of the spin-orbit coupling. This spin-orbit EFG (SO-EFG) is of interest in connection with relativistic effects in the magnetism of transition metals. The SO-EFG was first detected for Ir as a dilute impurity in Fe and Ni.[1–4] The interpretation as a spin-orbit effect has been worked out in Refs. 1, 2, 5 and 6.

Although the SO-EFG has been a long known effect, it has been determined so far only for a few systems,[7–11] mainly because the splitting of the magnetic resonance into a set of equidistant subresonances induced by the SO-EFG is relatively small. This quadrupole splitting is therefore usually hidden by the inhomogeneous broadening of the magnetic hyperfine splitting. The introduction of the MAPON (modulated adiabatic fast passage on oriented nuclei) technique,[12,13] however, has recently solved this experimental problem: Using MAPON, quadrupole splittings much smaller than the inhomogeneous broadening of the magnetic hyperfine splitting can be determined. Furthermore, MAPON measures directly the distribution of the quadrupole splitting in the sample. This is an essential improvement, since the SO-EFG shows a strong tendency to inhomogeneous broadening. A further shortcoming of previous studies was the complete neglect of the strong dependence of the SO-EFG on the direction of the magnetization with respect to the crystallographic axes. Although this anisotropy of the SO-EFG was theoretically predicted some time ago,[6] it has only recently been demonstrated experimentally for IrFe and PtFe.[11,14]

Due to these recent improvements a more systematic investigation of the SO-EFG has now become feasible. Here we report on MAPON measurements on the $5d$ impurities Pt, Ir, Os, and Re in cubic Co. The $5d$ impurities were chosen as the starting point, since there, as the consequence of a large spin-orbit coupling, the SO-EFG is considerably larger than for lighter impurities. The information on the SO-EFG in cubic Co so far has been particularly scarce: The EFG of AuCo(fcc) has been investigated with spin-echo nuclear magnetic resonance (NMR);[15] the sign of the EFG however could not be determined and the quadrupole splitting in the NMR spectrum could not be resolved, making the interpretation of the spectrum somewhat ambiguous. The EFG of CoCo(fcc) has been investigated with MAPON,[16] but the EFG proved to be inhomogeneously broadened by more than 100%. In this situation an accurate determination of the quadrupole splitting is impossible even with MAPON. (The implications of this large inhomogeneous broadening for the interpretation of the MAPON spectrum have in our opinion not been adequately taken into account in Ref. 16.) More information is available for the SO-EFG in hexagonal Co. In this case a peculiar pattern was found in the systematics of the SO-EFG: Whereas the SO-EFG of IrCo(hcp) is remarkably large, the SO-EFG of Pt, Au, and Hg is consistent with zero.[17]

II. MEASUREMENT OF SMALL QUADRUPOLE SPLITTINGS

In the hyperfine interaction in Fe, Co, and Ni the electric quadrupole interaction is superimposed on a much larger magnetic hyperfine interaction. This causes a splitting of the magnetic resonance of a nuclear state with spin I into $2I$ subresonances with equidistant subresonance separation $\Delta\nu_Q$. The frequency of the transition between the nuclear sublevels with magnetic quantum numbers m and $m+1$ is given by

$$\nu_{m\to m+1} = \nu_m - \Delta\nu_Q(m+\tfrac{1}{2}), \tag{1}$$

$$\nu_m = |g\mu_N(\vec{B}_{\mathrm{HF}} + \vec{B}_{\mathrm{ext}})/h|, \tag{2}$$

$$\Delta\nu_Q = \frac{3}{2I(2I-1)}\frac{eQV_{zz}}{h}, \tag{3}$$

where g is the nuclear g factor, eQ is the nuclear spectroscopic quadrupole moment, B_{HF} is the hyperfine field, B_{ext} is the external magnetic field, and V_{zz} is the zz component of the EFG tensor. The z direction is given by the sum of $\vec{B}_{\mathrm{HF}}$ and $\vec{B}_{\mathrm{ext}}$. Equations (1)–(3) are valid if the sublevels are

 ©2001 The American Physical Society

eigenfunctions of I_z. In the limit $\nu_m \gg \Delta\nu_Q$, which here should be a very good approximation, this holds irrespective of the form of the EFG tensor. This also means that only one component of the EFG tensor V_{zz} is accessible to the experiment. Therefore in the following we will refer to V_{zz} briefly as the EFG.

The technique of nuclear magnetic resonance on oriented nuclei (NMR-ON) is well suited to measure the hyperfine interaction of dilute impurities in ferromagnetic host lattices: The samples containing the radioactive impurities of interest are cooled to temperatures near 10 mK, where the nuclear spins become oriented with respect to the direction of the hyperfine field. This orientation leads to an anisotropic emission of the γ radiation. The interaction of the nuclear spin system with the radio frequency (rf) field is then detected via changes in the γ anisotropy. If the subresonance separation $\Delta\nu_Q$ is larger than the inhomogeneous broadening Γ_m of the magnetic hyperfine splitting, the individual subresonances are well resolved, and $\Delta\nu_Q$ can be directly determined from the NMR-ON spectrum.

If the subresonance structure is not resolved in the NMR-ON spectrum, the MAPON technique can be applied.[12,13] MAPON is an extension of the adiabatic fast passage (AFP) technique, where the rf frequency is swept over the resonance in a time that is short with respect to the nuclear spin-lattice relaxation time. In MAPON *two* rf frequencies with fixed frequency separation $\Delta\nu$ are swept over the resonance. In the presence of $2I$ subresonances split by the quadrupole interaction there is little change in the sublevel populations for $\Delta\nu < \Delta\nu_Q$ and large changes for $\Delta\nu > \Delta\nu_Q$. The magnitude of $\Delta\nu_Q$ can thus be obtained from the MAPON spectrum, which is the γ anisotropy after the MAPON sweep measured as a function of $\Delta\nu$. Since the magnetic hyperfine splitting does not enter, the method is independent of the corresponding inhomogeneous broadening. Usually the quadrupole splitting is also inhomogeneously broadened. Then the MAPON spectrum is, apart from some constants, the integral of the distribution $P(\Delta\nu_Q)$. In most cases $P(\Delta\nu_Q)$ can be well described by a Gaussian distribution. Center $\Delta\nu_Q^{(0)}$ and width $\Gamma_{\Delta\nu_Q}$ are obtained via a least squares fit of the integral over this distribution to the MAPON spectrum. $\Delta\nu_Q^{(0)}$ is interpreted as the subresonance separation, which would be found in a perfect sample.

The sign of the quadrupole splitting can be obtained by comparing the time dependence of the γ anisotropy after the sweep for both sweep directions. For an AFP sweep or MAPON sweep with $\Delta\nu > |\Delta\nu_Q|$ there is a characteristic difference (sweep asymmetry) depending only on the sign of $\Delta\nu_Q$ and the sweep direction: For positive $\Delta\nu_Q$ the relaxation back to equilibrium is faster (and the change in the γ anisotropy often larger) for sweep down than for sweep up. The reverse is true for negative $\Delta\nu_Q$.

The MAPON results were also used to interpret the NMR-ON spectra with unresolved quadrupole splitting as the superposition of strongly overlapping subresonances. In this way a more precise value of the magnetic hyperfine splitting can be obtained, provided that the quadrupole splitting is known from the MAPON measurement and the relative subresonance amplitudes are calculated as outlined in Ref. 18.

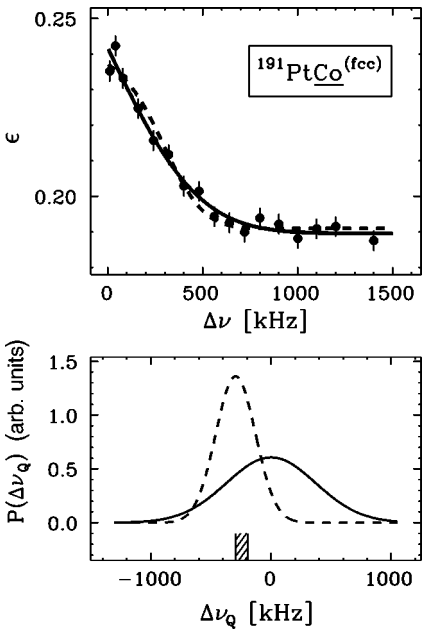

FIG. 1. Top: ^{191}Pt MAPON spectrum at $B_{ext}=0.5$ T. The data can be well described by a broad range of $\Delta\nu_Q^{(0)}$. The two extremes are (i) $\Delta\nu_Q^{(0)}=0$, $\Gamma_{\Delta\nu_Q}=874$ kHz (solid line) and (ii) $\Delta\nu_Q^{(0)}=-295$ kHz, $\Gamma_{\Delta\nu_Q}=390$ kHz (dashed line), respectively. Bottom: The distribution $P(\Delta\nu_Q)$ in cases (i) and (ii). Although the MAPON spectra for (i) and (ii) are practically indistinguishable the fraction f_r of the nuclei with the reverse sign of $\Delta\nu_Q$ is strongly different: 50% for (i), 3.7% for (ii). By combining MAPON and AFP data the range possible for $\Delta\nu_Q^{(0)}$ can be confined to the shaded frequency region.

In MAPON experiments on impurities in cubic Fe, Co, or Ni the difficulty that the inhomogeneous broadening of the quadrupole splitting considerably exceeds 100% arises quite often[11,16,19–21] and an accurate determination of $\Delta\nu_Q^{(0)}$ from the MAPON spectrum is then impossible. Since the implications of this situation for the interpretation of the MAPON spectrum have been largely ignored so far, they will be discussed here in some detail.

The difficulties arise because in MAPON both signs of $\Delta\nu_Q$ are projected onto the positive $\Delta\nu$ axis. The MAPON effect $\epsilon(\Delta\nu)$ is thus given by

$$\epsilon(\Delta\nu)=c_0+\int_0^{\Delta\nu}[c_1P(\Delta\nu_Q)+c_2P(-\Delta\nu_Q)]d\Delta\nu_Q, \tag{4}$$

where c_0, c_1, and c_2 are constants. Since the weighting of positive and negative $\Delta\nu_Q$ with c_1 and c_2 is in many cases not very different, the MAPON spectrum is essentially the integral over $P(\Delta\nu_Q)+P(-\Delta\nu_Q)$. This function turns out to be very insensitive to $\Delta\nu_Q^{(0)}$ if $\Gamma_{\Delta\nu_Q} \geqslant 1.3\,|\Delta\nu_Q^{(0)}|$. For the example ^{191}Pt*Co*(fcc) Fig. 1 illustrates that a broad range of $(\Delta\nu_Q^{(0)},\ \Gamma_{\Delta\nu_Q})$ pairs including $\Delta\nu_Q^{(0)}=0$ can describe the

spectrum equally well and only an upper limit for $|\Delta\nu_Q^{(0)}|$ can be deduced from the MAPON spectrum.

In principle a more accurate determination of $\Delta\nu_Q^{(0)}$ is possible if the sweep asymmetry is also taken into account: As can be seen from Fig. 1, the two distributions $P(\Delta\nu_Q)$ resulting in very similar MAPON spectra differ considerably in the extent to which $P(\Delta\nu_Q)$ contains both signs of the quadrupole splitting. Therefore $\Delta\nu_Q^{(0)}$ can be determined with moderate precision from the MAPON spectrum, if independent information is available for the parameter f_r, defined as the fraction of the nuclei with the less frequent sign of the quadrupole splitting. Since a nonzero value of f_r will reduce the sweep asymmetry, f_r can be determined along with the relaxation constant and the adiabatic factor A from a least squares fit to the time dependence of the γ anisotropy after sweep up and sweep down (MAPON or AFP).

Unfortunately, in practice the quantitative interpretation of the postpassage signal is subject to systematic errors arising mainly from temperature changes during the measurement: The rf power is applied only during the sweep to prevent a too strong heating of the sample by nonresonant absorption of rf power. Thus there is a sudden increase in temperature during the sweep and a subsequent cooling until the next sweep. This will diminish the true MAPON (AFP) effect and introduce an additional change in the γ anisotropy, which is insensitive to the sign of $\Delta\nu_Q$. In this way the sweep asymmetry can be considerably reduced. A quantitative treatment, however, is difficult because the time dependence of the temperature is not known with sufficient accuracy. (This clearly demonstrates the advantages of the MAPON method, which is independent of the exact form of the postpassage signal.) It is however possible to infer at least a reliable upper limit for f_r from the sweep asymmetry in the following way: The maximum sweep anisotropy would be found for $f_r=0$, $A\gg1$ and no temperature changes during the measurement. With respect to this maximum anisotropy the actual anisotropy is reduced, because $f_r>0$, the adiabatic factor A does not fulfill $A\gg1$, and/or because of the temperature rise during the sweep. If we neglect the temperature variation and assume $A\gg1$ in the theoretical description of the postpassage signal the whole asymmetry reduction is put into the parameter f_r and we obtain an upper limit for f_r from a least squares fit to the actual postpassage signal. Using this upper limit in the interpretation of the MAPON spectrum we obtain a lower limit for $|\Delta\nu_Q^{(0)}|$. In this way $|\Delta\nu_Q^{(0)}|$ can be delimited: An upper limit is deduced from the MAPON spectrum alone, and a lower limit can be deduced from the MAPON spectrum in combination with an upper limit for f_r from the sweep asymmetry.

III. EXPERIMENTAL DETAILS

In the preparation of the fcc Co samples care was taken to suppress the formation of hcp Co, which is the stable Co phase below $\approx$420 °C. 2-μm-thick Co foils purchased from Goodfellow Ltd. (purity 99.9%) were electrically heated for about 4 min to $\approx$1100 °C in high vacuum ($p<10^{-7}$ mbar). Then they were quenched to room temperature within <1 s. The high temperature and the rapid quenching proved to be essential for minimizing the content of hcp Co. The hcp Co content of the samples was determined by the intensity of the characteristic x-ray deflections to be less than 5% directly after the heat treatment and about 20% after the recoil implantations. In this work only the hyperfine interaction in the fcc phase was investigated. Contributions from the hcp phase can be definitely ruled out, since in all cases the resonance frequencies in hcp Co[21–23] are well outside the frequency range of the NMR-ON, MAPON, and AFP measurements.

A direct indicator for the structural quality of the fcc phase in the immediate vicinity of the probe nuclei is the linewidth of the NMR-ON resonance. In the experiments on ^{191}Pt, ^{186}Ir, and ^{182}Re the relative width of the magnetic hyperfine splitting was found to be $\Gamma_m/\nu_m=3.6(5)\times10^{-3}$, $1.5(4)\times10^{-3}$, and $4.0(1.3)\times10^{-3}$, respectively. This is only slightly larger than the linewidths found in coldrolled Fe and Ni foils of high purity. (The linewidth of the ^{183}Os resonance is almost completely due to the quadrupole splitting. The pure magnetic linewidth can therefore not be deduced from the NMR-ON spectrum.)

For the production of the $5d$ impurities the recoil implantation technique was employed: A stack of eight target foils (of natural Os, Re, or W to implant the Pt, Ir, or Os isotopes) each followed by a Co(fcc) foil was irradiated with α particles. The probe nuclei are produced in the target foils by (α,xn) reactions. Their kinetic energy is sufficient to implant the nuclei produced in the rear part of the target foil into the surface layer of the next Co(fcc) foil within a thickness of ≈0.2 μm. To implant ^{191}Pt ($I^\pi=3/2^-$, $T_{1/2}=2.9$ d) the reaction ^{192}Os$(\alpha,5n)^{191}$Pt ($E_\alpha\approx55$ MeV) was used. ^{186}Ir ($I^\pi=5^+$, $T_{1/2}=15.8$ h) and ^{188}Ir ($I^\pi=1^-$, $T_{1/2}=40.5$ h) were implanted via the reactions ^{185,187}Re$(\alpha,3n)^{186,188}$Ir ($E_\alpha\approx40$ MeV). The Os isotopes ^{181,182,183}Os were recoil implanted via the reactions ^{182,183,184}W$(\alpha,5n)^{181,182,183}$Os ($E_\alpha\approx55$ MeV). ^{183}Os ($I^\pi=9/2^+$, $T_{1/2}=13$ h) was used for the NMR-ON measurements on Os*Co*(fcc). The measurements on Re*Co*(fcc) were performed on the decay products of ^{181}Os and ^{182}Os, ^{181}Re ($I^\pi=5/2^+$, $T_{1/2}=20$ h), and ^{182}Re ($I^\pi=2^+$, $T_{1/2}=12.7$ h). All α irradiations were carried out at the cyclotron in Karlsruhe.

After the implantation the Co(fcc) foils were soldered with GaIn eutecticum to the Cu coldfinger, loaded into a ^{3}He-^{4}He dilution refrigerator (model TL-400 from Oxford Instruments) and cooled down to temperatures around 10 mK. The γ radiation was detected with four Ge detectors placed at 0°, 90°, 180°, and 270° with respect to the direction of the external magnetic field used to magnetize the sample. The γ anisotropy ϵ is defined as the following ratio of the different count rates W:

$$\epsilon=\frac{W(0°)+W(180°)}{W(90°)+W(270°)}-1. \tag{5}$$

The temperature was measured with a ^{60}Co*Co*(hcp) nuclear orientation thermometer.

The frequency spectrum for the MAPON measurements with two frequencies separated by $\Delta\nu$ was obtained by mixing the frequency of a rf synthesizer (Marconi, model 2031) with a modulation frequency $\Delta\nu/2$ from an audio frequency function generator, using a double-balanced mixer. With respect to the two main components other components in the frequency spectrum were suppressed by more than 30 dB. For the MAPON (or AFP) measurements a linear voltage sweep was applied to the external modulation input of the synthesizer. The voltage sweep was supplied by an integrator circuit with adjustable time constant. For the NMR-ON measurements the frequency was doubly frequency modulated: 100 Hz with bandwidth between ± 0.3 and ± 1 MHz, and 1 Hz with bandwidth ± 100 Hz. (In this way it is assured that the splitting of the spectrum by the modulation in discrete Fourier components is finer than the power broadening and the stability of the rf generator and is thus smoothed out.) For each frequency the γ anisotropy was measured with and without frequency modulation and the difference of both anisotropies was analyzed.

IV. MEASUREMENTS

A. ^{191}Pt*Co*(fcc)

Besides the SO-EFG of Pt*Co*(fcc) the following aspect of the hyperfine interaction specific to the isotope ^{191}Pt was also investigated: For magnetic fields $B_{\rm ext}<0.4$ T the ^{191}Pt resonance happens to partly overlap the resonance frequency of stable ^{59}Co. It is known that in this case the static and/or dynamic hyperfine interaction of impurity nuclei can be affected by a coupling to the nuclear spin waves.[24] The nuclear spin waves are collective excitations of the ^{59}Co nuclear spin system, which arise at low temperatures through the coupling of the nuclear spins via the Suhl–Nakamura interaction.[25] Actually we found an increase of the nuclear spin–lattice relaxation (NSLR) of ^{191}Pt by 2 orders of magnitude due to this effect. A detailed discussion of this aspect of the experiment is given in Ref. 26.

The static hyperfine interaction, however, seemed not to be affected: Although the NSLR changed dramatically, the position and the width of the ^{191}Pt resonance remained essentially constant between 10 mT and 1 T apart from the usual resonance shift with the external field. The resonance frequency $\bar{\nu}$ in zero field was deduced to be 203.14(7) MHz.[26] Taking the quadrupole splitting into account we obtain the magnetic hyperfine splitting in zero field:

$$\nu_m(^{191}\mathrm{Pt}Co(\mathrm{fcc}), B_{\rm ext}=0)=202.93(9)\ \ \mathrm{MHz}.$$

To avoid any complications from the influence of the nuclear spin waves the MAPON measurements were performed at $B_{\rm ext}=0.5$ T (sweep region 199.3–204.3 MHz, duration of MAPON sweep 1 s, sweep down). Figure 1 shows the ^{191}Pt MAPON spectrum. It is a typical example of the situation $\Gamma_{\Delta\nu_Q}>\Delta\nu_Q^{(0)}$. The spectrum can be well described by any $|\Delta\nu_Q^{(0)}|$ between 0 and 295 kHz. To deduce the sign of $\Delta\nu_Q^{(0)}$ the AFP postpassage signal had to be measured, since for $I=3/2$ the final state after the MAPON sweep is nearly independent of the sweep direction. The AFP data (Fig. 2) demonstrate that the sign of the quadrupole splitting is negative for the majority of the ^{191}Pt nuclei.

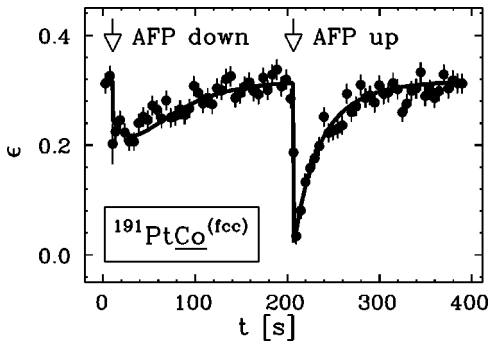

FIG. 2. ^{191}Pt AFP postpassage signal for both sweep directions, $B_{\rm ext}=0.5$ T. Although the data can be well described by $f_r=0$ (solid line), the Korringa constant $C_K=0.60(4)$ Ks obtained in this way deviates from $C_K=0.22(2)$ Ks measured in the same experiment with NMR-ON (Ref. 26). This failure of our description is presumably due to neglecting the temperature variations during the AFP measurement. But even without detailed knowledge of these temperature variations one can obtain at least a reliable upper limit for f_r by analyzing the AFP data with the assumption $A\gg 1$ for the adiabatic factor. From the data shown here we obtain $f_r\leqslant 0.26(2)$.

From the quantitative analysis of the AFP data with the restriction $A\gg 1$ we obtain as an upper limit $f_r<28\%$. With this information we obtain from the MAPON spectrum a lower limit for $|\Delta\nu_Q^{(0)}|$ and get as the final result:

$$-295\ \ \mathrm{kHz}<\Delta\nu_Q^{(0)}(^{191}\mathrm{Pt}, B_{\rm ext}=0.5\ \ \mathrm{T})<-195\ \ \mathrm{kHz}.$$

B. ^{186,188}Ir*Co*(fcc)

With the resonance frequency of ^{192}Ir in fcc Co from Ref. 4 and the known ratio of the resonance frequencies of ^{186}Ir and ^{192}Ir in Ni[18,27] the ^{186}Ir resonance can be calculated to be at 551.9(4.2) MHz for $B_{\rm ext}=0.1$ T, the error originating mainly from the unknown quadrupole splitting. The actual position of the ^{186}Ir resonance, $\bar{\nu}=550.35(3)$ MHz at $B_{\rm ext}=0.1$ T, agrees well with this prediction. Fig. 3 shows the

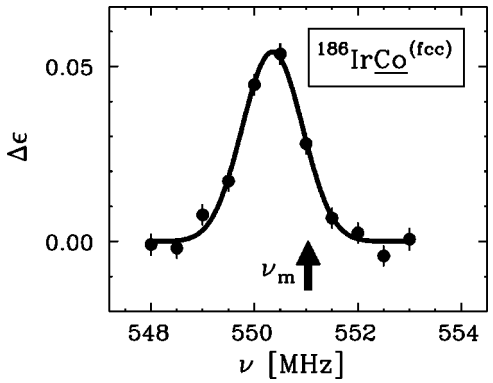

FIG. 3. NMR-ON spectrum of ^{186}Ir for $B_{\rm ext}=0.1$ T. $T\approx 26$ mK. Modulation bandwidth $\Delta\nu^{\rm rf}=\pm 0.5$ MHz. The arrow marks the position of the magnetic resonance frequency, as reconstructed with the help of the MAPON results.

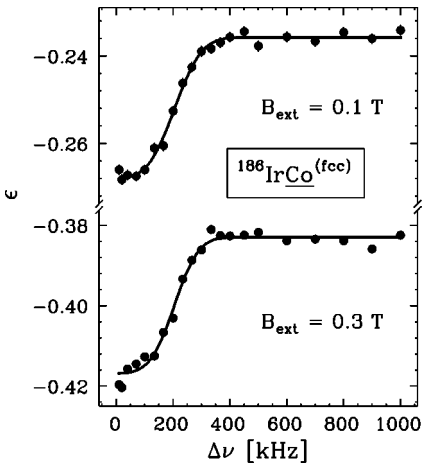

FIG. 4. MAPON spectrum of ^{186}Ir for two magnetic fields.

NMR-ON spectrum. Taking the external magnetic field and the quadrupole splitting into account we obtain

$$\nu_m(^{186}\mathrm{Ir}Co(\mathrm{fcc}),B_{\mathrm{ext}}=0)=551.62(13)\ \ \mathrm{MHz}.$$

The quadrupole splitting was measured with MAPON for $B_{\mathrm{ext}}=0.1$ and 0.3 T (sweep range 547.5–558.5 MHz for $B_{\mathrm{ext}}=0.1$ T, 546.8–554.8 MHz for $B_{\mathrm{ext}}=0.3$ T, duration of sweep 0.05 s, sweep up). Figure 4 shows both MAPON spectra. The short sweep time was necessary because of the short nuclear relaxation time. The positive sign of the quadrupole splitting was determined from the asymmetry between AFP sweep up and sweep down (Fig. 5). The deduced quadrupole splittings are

$$\Delta\nu_Q^{(0)}(^{186}\mathrm{Ir},B_{\mathrm{ext}}=0.1\ \ \mathrm{T})=+213(9)\ \ \mathrm{kHz},$$

$$\Delta\nu_Q^{(0)}(^{186}\mathrm{Ir},B_{\mathrm{ext}}=0.3\ \ \mathrm{T})=+213(9)\ \ \mathrm{kHz}.$$

The relative width of $P(\Delta\nu_Q)$ is 83(8)% and 74(10)% for 0.1 and 0.3 T, respectively.

The $\Delta\nu_Q^{(0)}$'s given above are already corrected for rf power broadening. As discussed in Ref. 13 the power broadening contributes to the width of the MAPON spectrum and in general also causes a small shift, which can be estimated by model calculations.[13,21] For the two MAPON measurements on ^{186}Ir the shift $\delta\Delta\nu_Q$ was estimated to be $-7(7)$ and $-6(6)$ kHz for 0.1 and 0.3 T, respectively, which is of the same order of magnitude as the statistical error. (These estimates are rather inaccurate because only the order of magnitude of the adiabatic parameter is known reliably.) In most cases the power broadening can be safely neglected with respect to the experimental error. This does not apply here because of the short sweep time: For a given adiabatic parameter the power broadening is proportional to $\sqrt{d\nu/dt}$, the square root of the sweep rate.

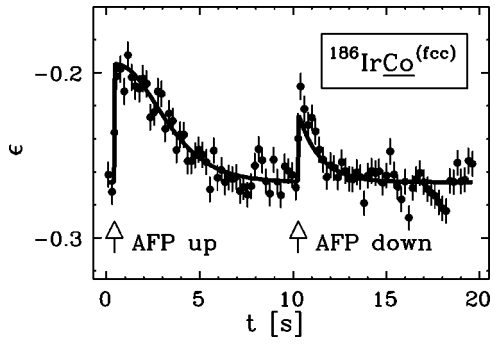

FIG. 5. Asymmetry in the AFP postpassage signal for ^{186}Ir, $B_{\mathrm{ext}}=0.1$ T. The slight deviations here and in Fig. 9 between the data and the theoretical description (solid line) may be due to temperature variations not taken into account by the theory.

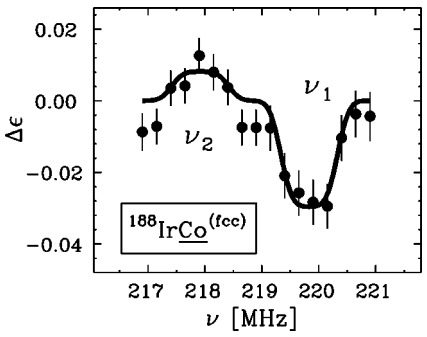

FIG. 6. NMR-ON spectrum of ^{188}Ir for $B_{\mathrm{ext}}=0.3$ T. $\Delta\nu^{\mathrm{rf}}=\pm0.5$ MHz. For the nuclear spin $I=1$ of ^{188}Ir the NMR-ON spectrum consists of two subresonances, ν_1 and ν_2, the amplitudes having opposite signs.

NMR-ON measurements were also performed for ^{188}Ir. Here the quadrupole splitting is resolved due to the low spin ($I=1$) of this isotope. Because of the low intensity of the 2214 keV γ transition, which is the transition most suitable for NMR-ON, only one NMR–ON spectrum could be measured (Fig. 6). From this spectrum we deduce the following hyperfine splitting frequencies:

$$\nu_m(^{188}\mathrm{Ir}Co(\mathrm{fcc}),B_{\mathrm{ext}}=0)=219.56(10)\ \ \mathrm{MHz},$$

$$\Delta\nu_Q^{(0)}(^{188}\mathrm{Ir},B_{\mathrm{ext}}=0.3\ \ \mathrm{T})=-1.92(20)\ \ \mathrm{MHz}.$$

The following ratios between the ^{188}Ir and the ^{186}Ir hyperfine splitting frequencies in fcc Co can be deduced from our data:

$$\Delta\nu_Q(^{188}\mathrm{Ir})/\Delta\nu_Q(^{186}\mathrm{Ir})=-9.0(1.0),$$

$$\nu_m(^{188}\mathrm{Ir})/\nu_m(^{186}\mathrm{Ir})=0.398\,03(20).$$

These are in perfect agreement with the more precisely known ratios for hcp Co:[22]

$$\Delta\nu_Q(^{188}\mathrm{Ir})/\Delta\nu_Q(^{186}\mathrm{Ir})=-8.518(32),$$

$$\nu_m(^{188}\mathrm{Ir})/\nu_m(^{186}\mathrm{Ir})=0.398\,06(5).$$

C. ^{183}Os, ^{181,182}ReCo(fcc)

The ^{183}OsCo(fcc) resonance could be predicted within 2% from the known hyperfine field.[28] A NMR-ON spectrum for ^{183}Os was measured for $B_{\mathrm{ext}}=0.1$ T (Fig. 7). The center and the width of the resonance were found to be 119.59(11) and 1.8(3) MHz, respectively. Although the quadrupole split-

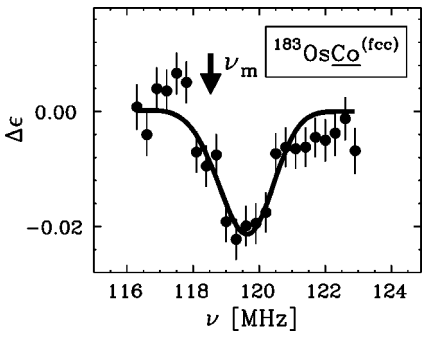

FIG. 7. NMR-ON spectrum of ^{183}Os for $B_{\rm ext}=0.1$ T. $T\approx 12$ mK. $\Delta\nu^{\rm rf}=\pm 0.3$ MHz.

ting is not resolved in the NMR-ON spectrum it considerably shifts the resonance center and is the dominant contribution to the linewidth. Taking the quadrupole splitting into account we deduce $\nu_m=118.53(28)$ MHz and extrapolating to zero field we obtain:

$$\nu_m(^{183}\mathrm{Os}Co(\mathrm{fcc}),B_{\rm ext}=0)=118.66(28)\ \ \mathrm{MHz}.$$

MAPON measurements on ^{183}Os were performed for $B_{\rm ext}=0.1$, 0.3, and 0.5 T (sweep from 115.6 to 121.6 MHz, 117.3 to 121.3 MHz, and 115.6 to 121 MHz for 0.1, 0.3, and 0.5 T, respectively, sweep time 0.5 s, sweep up). The MAPON spectra are shown in Fig. 8. The following quadrupole splittings are deduced:

$$\Delta\nu_Q^{(0)}(^{183}\mathrm{Os},B_{\rm ext}=0.1\ \ \mathrm{T})=-420(17)\ \ \mathrm{kHz},$$

$$\Delta\nu_Q^{(0)}(^{183}\mathrm{Os},B_{\rm ext}=0.3\ \ \mathrm{T})=-372(17)\ \ \mathrm{kHz},$$

$$\Delta\nu_Q^{(0)}(^{183}\mathrm{Os},B_{\rm ext}=0.5\ \ \mathrm{T})=-354(10)\ \ \mathrm{kHz}.$$

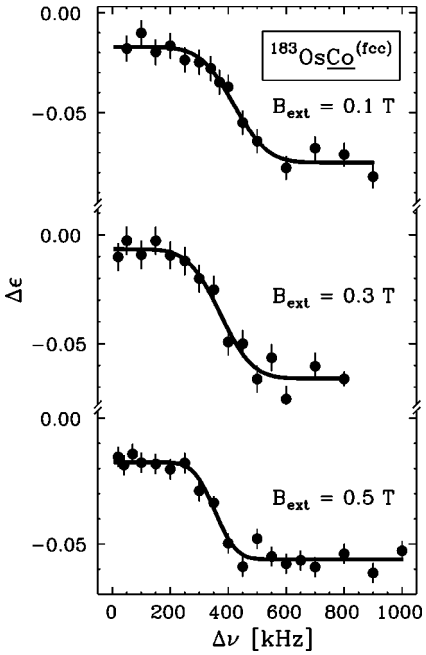

FIG. 8. MAPON spectrum of ^{183}Os for different magnetic fields.

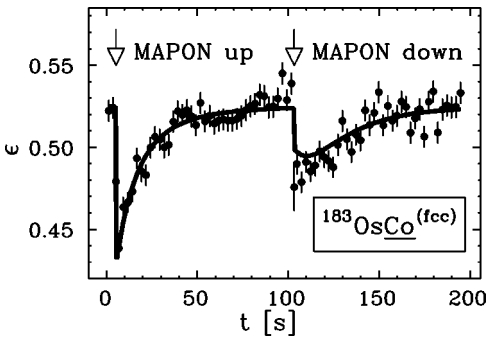

FIG. 9. ^{183}Os MAPON postpassage signal for both sweep directions, $B_{\rm ext}=0.5$ T.

The negative sign of $\Delta\nu_Q^{(0)}$ was obtained from the asymmetry in the MAPON postpassage signal between sweep up and down (Fig. 9). $\Gamma_{\Delta\nu_Q}/\Delta\nu_Q^{(0)}$ was found to be 51(13)%, 55(14)%, and 39(11)% for 0.1, 0.3, and 0.5 T.

After completion of the measurements on ^{183}Os the hyperfine interaction of ^{181}Re and ^{182}Re was investigated. At $B_{\rm ext}=0.1$ T the ^{181}Re resonance was searched in the range from 400 to 500 MHz. According to the hyperfine field of ReCo from Ref. 28 the resonance was expected to be around 430 MHz, however a significant ^{181}Re signal was found only at $\approx$470 MHz (no ^{182}Re signal was observed in this frequency region). The ^{182}Re resonance could then be accurately predicted. Figure 10 shows the ^{181}Re and ^{182}Re NMR-ON spectra. The resonance centers are 469.95(26) and 620.97(16) MHz for ^{181}Re and ^{182}Re, respectively. Taking into account the quadrupole splitting and extrapolating to zero magnetic field we obtain

$$\nu_m(^{181}\mathrm{Re}Co(\mathrm{fcc}),B_{\rm ext}=0)=471.26(38)\ \ \mathrm{MHz},$$

$$\nu_m(^{182}\mathrm{Re}Co(\mathrm{fcc}),B_{\rm ext}=0)=622.70(49)\ \ \mathrm{MHz}.$$

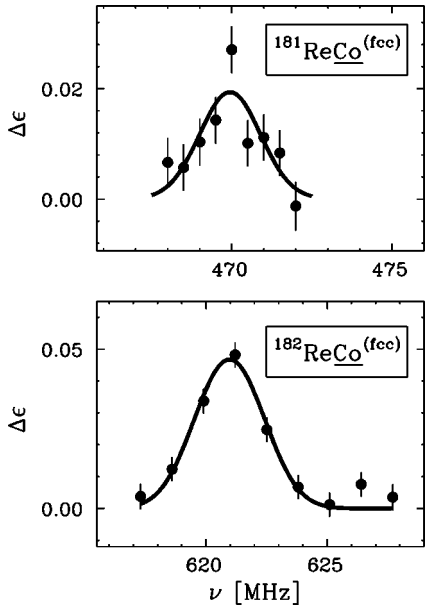

FIG. 10. NMR-ON spectra of ^{181}Re (top) and ^{182}Re (bottom) for $B_{\rm ext}=0.1$ T. $\Delta\nu^{\rm rf}=\pm 0.5$ MHz (top), $=\pm 1.3$ MHz (bottom).

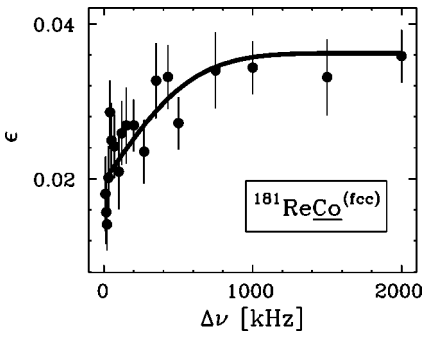

FIG. 11. MAPON spectrum of ^{181}Re, $B_{ext}=0.1$ T.

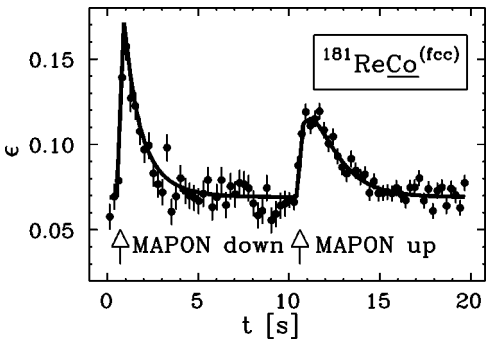

FIG. 12. ^{181}Re MAPON postpassage signal for $\Delta\nu>\Delta\nu_Q$ in both sweep directions, $B_{ext}=0.1$ T.

The resulting ratio of the hyperfine splittings,

$$\nu_m(^{182}\mathrm{Re})/\nu_m(^{181}\mathrm{Re})=1.3214(15),$$

is in good agreement with the ratio 1.3228(16), which can be deduced from the resonance frequencies of ^{181,182,183}Re in Fe and Ni from Refs. 21, 29, and 30.

The quadrupole splitting of ^{181}Re was measured with MAPON for $B_{ext}=0.1$ T, the rf frequency was swept from 464 to 476 MHz in 0.4 s. The MAPON spectrum is shown in Fig. 11. The MAPON postpassage signal for $\Delta\nu>\Delta\nu_Q$ was also measured for sweep down, and it is compared with the sweep up signal in Fig. 12. The asymmetry between both sweep directions shows unambiguously that the quadrupole splitting is predominantly positive. There is however no clearly defined transition region in the MAPON spectrum from $\Delta\nu<\Delta\nu_Q$ to $\Delta\nu>\Delta\nu_Q$. As discussed in Sec. II, this happens if the inhomogeneous width of $P(\Delta\nu_Q)$ is considerably larger than 100%. In this situation only upper and lower limits for the center $\Delta\nu_Q^{(0)}$ of $P(\Delta\nu_Q)$ can be obtained from the quantitative analysis of MAPON spectrum and sweep asymmetry. In this way we obtain for ^{181}Re:

$$+80\ \mathrm{kHz}<\Delta\nu_Q^{(0)}(^{181}\mathrm{Re},B_{ext}=0.1\ \mathrm{T})<+480\ \mathrm{kHz}.$$

V. RESULTS AND DISCUSSION

From $\nu_m(B_{ext}=0)$ we can deduce the hyperfine fields of Pt, Ir, Os, and Re in Co(fcc), which are listed in Table I. The following g factors were used: $g(^{191}\mathrm{Pt})=0.329(5)$,[31] $g(^{186}\mathrm{Ir})=0.759(24)$,[27] $g(^{183}\mathrm{Os})=0.1786(31)$ (Ref. 32, recalculated with $\nu_m(^{183}\mathrm{Os}Fe)=151.6(2)$ MHz[21] in zero field), and $g(^{181}\mathrm{Re})=1.277(5)$ (Ref. 30, recalculated with $B_{HF}(^{183}\mathrm{Re}Fe)=-74.94(28)$ T[29]). The hyperfine fields of Pt, Ir, Os, and Re in Co had already been obtained with spin-echo NMR by Kontani and Itoh.[28] These hyperfine fields are also listed in Table I. However it is not clear whether the hyperfine fields quoted in Ref. 28 refer to the fcc or hcp phase of Co, although in most cases it will be the fcc phase. For PtCo(fcc) and OsCo(fcc) the hyperfine fields deduced in this work and in Ref. 28 agree within the experimental error. For IrCo(fcc) there is a discrepancy, which can however be interpreted as the hyperfine anomaly between ^{193}Ir, which has a large single level hyperfine anomaly, and ^{186}Ir. This is supported by the fact that the ratios between the magnetic hyperfine splitting frequencies of ^{193}Ir and ^{186}Ir in Ni and Co(fcc), where the hyperfine anomaly should be about the same, agree within the experimental error: $\nu_{Co}^{186}/\nu_{Co}^{193}=6.65(14)$ (this work, Ref. 28) and $\nu_{Ni}^{186}/\nu_{Ni}^{193}=6.652(5)$ (Refs. 27 and 33). For ReCo(fcc) there is also a significant discrepancy of about 10%. A hyperfine anomaly of this order of magnitude between ^{183}Re and ^{185,187}Re is not expected. But meanwhile we have also determined the hyperfine field of ^{183}ReCo(hcp) in zero field to be 44.41(17) T.[21] Thus in Ref. 28 probably the hyperfine field of ReCo(hcp) was determined.

For the determination of a quantity, which is expected to be dependent on the direction of the magnetization with respect to the crystal axes, experiments on single crystals should be performed. However, these are not available for Co(fcc). Thus only the EFG averaged over different directions of the magnetization can be determined from polycrystal samples. The orientation of the crystal axes in our Co(fcc) foils was investigated by scanning the [111] x-ray reflection in a pole figure. No deviation from a completely random orientation of the crystal axes could be detected (in contrast to coldrolled Fe and Ni foils, where the pole figures revealed the presence of strong textures). For a uniform magnetization of the sample along $\vec{B}_{ext}$ at high fields (for our samples the γ anisotropy saturated around $B_{ext}=0.5$ T) this implies a random orientation of the magnetization with respect to the crystal axes. In zero field however the magnetization should be preferentially oriented along the easy axes ([111]). Thus the anisotropy of the SO-EFG may introduce a magnetic field dependence of the EFG in polycrystal samples. For IrCo(fcc) no significant magnetic field dependence was found. For OsCo(fcc) the quadrupole splitting for $B_{ext}=0.1$ T is slightly larger, which may point to a larger SO-EFG for $\vec{M}\|[111]$. For ReCo(fcc) the quadrupole splitting was measured only for $B_{ext}=0.1$ T. In this case, however, a possible slight magnetic field dependence can be neglected with respect to the large experimental error. For the derivation of $\langle V_{zz}\rangle$ for Pt, Ir, and Os only the results for $B_{ext}\geqslant 0.3$ T had been used. Thus $\langle V_{zz}\rangle$ given here can be interpreted as the SO-EFG averaged over all possible orientations

TABLE I. Hyperfine field and electric field gradient for Re, Os, Ir, Pt, and Au in cubic Co from this work and from spin-echo NMR (SE NMR) experiments.

Impurity	B_{HF} (T) (NMR-ON)	B_{HF} (T) (SE NMR)	$\langle V_{zz}\rangle$ (10^{16} V/cm^2)
Re	$-48.4(2)$[a] (^{181}Re)	$-43.6(9)$[b,c] (^{185,187}Re)	$+0.36(26)$[a]
Os	$-87.2(15)$[a] (^{183}Os)	$-85.8(17)$[b] (^{189}Os)	$-1.15(11)$[a]
Ir	$-95.3(30)$[a] (^{186}Ir)	$-102.7(20)$[b] (^{193}Ir)	$-1.04(5)$[a]
Pt	$-80.9(12)$[a] (^{191}Pt)	$-81.8(17)$[b] (^{195}Pt)	$+0.23(5)$[a]
Au		$-78.25(7)$[d] (^{197}Au)	$\pm 1.13(30)$[d]

[a]This work.
[b]Reference 28, recalculated with magnetic moments from Ref. 37.
[c]Probably $B_{HF}(\mathrm{Re}Co(\mathrm{hcp}))$.
[d]Reference 15.

of the cubic lattice relative to the direction of the magnetization.

To derive $\langle V_{zz}\rangle$ from the quadrupole splitting the following quadrupole moments were used: $Q(^{191}\mathrm{Pt}) = -0.87(4)$ b,[31] $Q(^{186}\mathrm{Ir}) = -2.548(31)$ b,[22] $Q(^{183}\mathrm{Os}) = +3.12(27)$ b,[34] and $Q(^{181}\mathrm{Re}) \approx Q(^{183}\mathrm{Re}) = +2.1(2)$ b[34] (within the experimental error ^{181}Re and ^{183}Re are expected to have the same quadrupole moment).[35] The average SO-EFG's in Co(fcc) deduced in this way are listed in Table I. They are shown as a function of the $5d$ impurity in Fig. 13.

$\langle V_{zz}\rangle(\mathrm{Au}Co(\mathrm{fcc}))$ from Ref. 15 is not shown in Fig. 13 since the sign is not known and also the absolute magnitude should be viewed with some caution: The quadrupole splitting was not clearly resolved in the spin-echo NMR spectrum and therefore the interpretation of the spectrum had to rely on some assumptions on the form of the inhomogeneous broadening of the magnetic and the quadrupole splitting.

The SO-EFG was determined until recently for only a small number of impurities because of the insufficient resolution of the measurement techniques available, and not because an appreciable SO-EFG exists only for a small number of impurities. This has already been suggested in Ref. 2 and is now confirmed by our measurements: The SO-EFG's of Ir and Os in Co(fcc) are of the same order of magnitude (10^{16} V/cm^2) as the well known SO-EFG's of Ir and Au in Fe and Ni. But our measurements also show that for some impurity host combinations like PtCo(fcc) the SO-EFG is nearly an order of magnitude smaller.

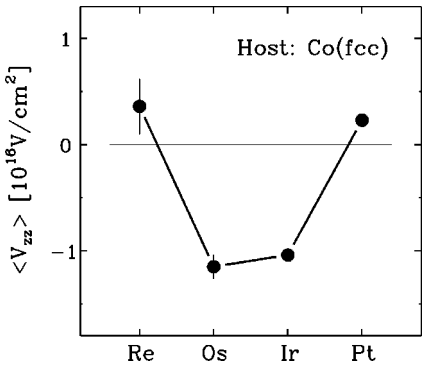

FIG. 13. Average SO-EFG in Co(fcc) for the $5d$ impurities.

One advantage of hyperfine interaction studies is the possibility of investigating the systematics of an effect on a continuous series of impurity elements. This now also becomes possible for the SO-EFG. The most conspicuous feature of the systematics in Fig. 13 is the strong impurity dependence. The variation of the SO-EFG with the atomic number of the impurity is of the same order of magnitude as the SO-EFG itself. A similar situation has recently been found for Fe as the host: The SO-EFG of Pt in Fe is drastically smaller than the SO-EFG's of the neighboring $5d$ elements Au and Ir.[11]

The physical reasons for the strong impurity dependence are: (i) The local magnetic and orbital moments change appreciably over the $5d$ impurity series. (ii) In contrast to the magnetic hyperfine interaction, which is dominated by the only slightly impurity dependent ''transferred hyperfine field,''[36] the SO-EFG is determined mainly by the local spin-orbit coupling. (iii) The SO-EFG, as an effect second order in the spin-orbit coupling, is more sensitive to band structure details than, for example, the local orbital moment, which is a first order effect.[5,21] The SO-EFG is thus an ideal quantity for studying the interplay between spin-orbit coupling and band structure, where the local band structure can be varied in a defined way via the impurity. Because of the large influence of the local band structure however we have to leave this interpretation of our data to future *ab initio* calculations. Spin-orbit contributions to the magnetic part of the hyperfine interaction have already been calculated,[36] but in this case a comparison with the experiment is difficult, since the contribution from the local orbital moment can usually not be separated from the much larger Fermi-contact field.

For Ir in hexagonal Co the average SO-EFG is $\langle V_{zz}\rangle = -3.78(7)\times 10^{16}$ V/cm^2,[17] about four times larger than in Co(fcc). In view of the similar lattice spacings, similar magnetization and similar magnetic hyperfine fields of the two Co phases, this is evidence for a remarkably strong sensitivity of the SO-EFG to the lattice symmetry.

To summarize, although the SO-EFG in Fe, Co, and Ni has been known for a long time, an experimental investigation of the systematics of this effect has become possible only recently due to the MAPON technique. We have measured the SO-EFG of Pt, Ir, Os, and Re in cubic Co. The same order of magnitude and a similar strong impurity de-

pendence is found for 5*d* impurities in Fe and Ni. Despite the similar magnetic properties of Co(fcc) and Co(hcp) the SO-EFG of Ir is strongly different in both Co phases. As a pure effect of the spin-orbit coupling the SO-EFG will be a sensitive test for the recently developed schemes for the incorporation of the spin-orbit coupling in band structure calculations.

ACKNOWLEDGMENTS

We wish to thank E. Smolic for experimental help. This work has been funded by the Deutsche Forschungsgemeinschaft (DFG) under Contract No. Ha 1282/3-3 and by the Forschungszentrum Karlsruhe GmbH.

[1] M. Aiga and J. Itoh, J. Phys. Soc. Jpn. **31**, 1844 (1971).
[2] M. Aiga and J. Itoh, J. Phys. Soc. Jpn. **37**, 967 (1974).
[3] R.L. Mössbauer, M. Lengsfeld, W. v. Lieres, W. Potzel, P. Teschner, F. E. Wagner, and G. Kaindl, Z. Naturforsch. A **26A**, 343 (1971).
[4] P. D. Johnston and N. J. Stone, J. Phys. C **5**, L303 (1972).
[5] G. A. Gehring and H. C. W. L. Williams, J. Phys. F: Met. Phys. **4**, 291 (1974).
[6] C. Demangeat, J. Phys. F: Met. Phys. **5**, 169 (1975).
[7] P. C. Riedi and E. Hagn, Phys. Rev. B **30**, 5680 (1984).
[8] J. J. Spijkerman, J. C. Travis, D. N. Pipkorn, and C. E. Violet, Phys. Rev. Lett. **26**, 323 (1971).
[9] H. Enokiya and M. Kawakami, J. Phys. Soc. Jpn. **50**, 2221 (1981).
[10] P. J. Back, D. H. Chaplin, and P. T. Callaghan, Phys. Rev. B **37**, 4911 (1988).
[11] G. Seewald, E. Hagn, E. Zech, R. Kleyna, M. Voß, D. Forkel-Wirth, A. Burchard, and ISOLDE Collaboration, Phys. Rev. Lett. **82**, 1024 (1999).
[12] P. T. Callaghan, P. J. Back, D. H. Chaplin, H. R. Foster, and G. V. H. Wilson, *Proceedings of the International Symposium on Nuclear Orientation and Nuclei far from Stability*, Hyperfine Interact. **22**, 39 (1985).
[13] P. T. Callaghan, P. J. Back, and D. H. Chaplin, Phys. Rev. B **37**, 4900 (1988).
[14] G. Seewald, E. Hagn, E. Zech, D. Forkel-Wirth, A. Burchard, and ISOLDE Collaboration, Phys. Rev. Lett. **78**, 1795 (1997).
[15] M. Kawakami, H. Enokiya, and T. Okamoto, J. Phys. F: Met. Phys. **15**, 1613 (1985).
[16] W. D. Hutchison, A. V. J. Edge, N. Yazidjoglou, and D. H. Chaplin, Phys. Rev. Lett. **67**, 3436 (1991).
[17] G. Seewald, B. Hinfurtner, E. Hagn, E. Zech, D. Forkel-Wirth, R. Eder, and ISOLDE Collaboration, Phys. Rev. Lett. **80**, 3638 (1998).
[18] E. Hagn, K. Leuthold, E. Zech, and H. Ernst, Z. Phys. A **295**, 385 (1980).
[19] D. H. Chaplin, W. D. Hutchison, M. P. Kopp, and N. Yazidjoglou, Hyperfine Interact. **43**, 241 (1988).
[20] N. Yazidjoglou, W. D. Hutchison, and G. A. Stewart, J. Phys.: Condens. Matter **6**, 7109 (1994).
[21] G. Seewald, Ph.D. thesis, TU München, 1999.
[22] G. Seewald, E. Hagn, B. Hinfurtner, E. Zech, D. Forkel-Wirth, R. Eder, and ISOLDE Collaboration, Phys. Rev. Lett. **77**, 5016 (1996).
[23] B. Hinfurtner, E. Hagn, E. Zech, R. Eder, and ISOLDE Collaboration, Phys. Rev. Lett. **64**, 2188 (1990).
[24] G. Seewald, E. Hagn, and E. Zech, Phys. Rev. Lett. **79**, 2550 (1997).
[25] P. G. de Gennes, P. Pincus, F. Hartmann-Boutron, and J. M. Winter, Phys. Rev. **129**, 1105 (1963).
[26] G. Seewald, E. Hagn, and E. Zech, Phys. Rev. Lett. **78**, 5002 (1997).
[27] E. Hagn and E. Zech, Z. Phys. A **297**, 329 (1980).
[28] M. Kontani and J. Itoh, J. Phys. Soc. Jpn. **22**, 345 (1967).
[29] S. Ohya, K. Nishimura, and N. Mutsuro, Hyperfine Interact. **36**, 219 (1987).
[30] E. Hagn and G. Eska, Nucl. Phys. A **363**, 269 (1981).
[31] Th. Hilberath, St. Becker, G. Bollen, H.-J. Kluge, U. Krönert, G. Passler, J. Rikovska, R. Wyss, and ISOLDE Collaboration, Z. Phys. A **342**, 1 (1992).
[32] E. Hagn and E. Zech, Z. Phys. A **295**, 345 (1980).
[33] M. Aiga, J. Itoh, and V. Saraswati, J. Phys. Soc. Jpn. **31**, 1843 (1971).
[34] E. Hagn, Hyperfine Interact. **22**, 19 (1985).
[35] C. Ekström, H. Rubinsztein, and P. Möller, Phys. Scr. **14**, 199 (1976).
[36] H. Ebert, R. Zeller, B. Drittler, and P. H. Dederichs, J. Appl. Phys. **67**, 4576 (1990).
[37] P. Raghavan, At. Data Nucl. Data Tables **42**, 189 (1989).